Parameter estimation of gravitational wave with various time-delay interferometry channels

Mengxu Liu* and Biping Gong

Physics Department, Huazhong University of Science and Technology, Wuhan 430074, China

(Received 20 July 2023; accepted 4 December 2023; published 27 December 2023)

Parameter estimation plays a critical role in the detection of gravitational waves, and for space-based detectors, time delay interferometry is indispensable to ensure mission success. This paper employs the Fisher matrix method to systematically analyze the parameter estimation and localization capabilities of TianQin and LISA for monochromatic sources and coalescing supermassive black hole binaries under various time-delay interferometry combinations. For monochromatic sources, the accuracy of parameter estimation for TianQin and LISA significantly improves within one year of observation time, followed by a gradual increase due to signal-to-noise ratio effects. The improvement in localization with multichannel data stabilizes at 2–4 times that of single-channel data after the observation time exceeds one year. The coalescence of supermassive black hole binaries is investigated by considering 30-day inspiral-merger-ringdown signals that incorporate higher-order modes. It is observed that the inclusion of higher modes enhances the localization advantages provided by a multichannel network. Specifically, for TianQin, the multichannel network yields significant improvements in localization accuracy for binaries with a total mass of $4 \times 10^6 M_\odot$, up to an order of magnitude. In contrast, for LISA, the gains increase with mass, ranging from several times at $2 \times 10^5 M_\odot$ to more than 2 orders of magnitude at $4 \times 10^7 M_\odot$.

DOI: 10.1103/PhysRevD.108.123042

I. INTRODUCTION

While the indirect verification of gravitational waves (GWs) was established through the observation of orbital period decay in binary stars during the 1970s, a significant milestone was achieved with the inaugural direct detection of GWs in 2015 [1–4]. This successful detection has engendered a profound surge in enthusiasm among researchers and experts, propelling them toward the ambitious goal of detecting GWs across the entire spectrum. So far nearly 100 medium and high frequency (10 Hz–10^3 Hz) GW events corresponding to merging signals of compact binaries have been detected by the ground-based detectors LIGO and Virgo [5,6]. The low-frequency signals (<1 Hz) from a wider range of GW sources cannot be detected on the ground because of a low-frequency noise wall composed of seismic noise and Newtonian noise. Currently the most feasible solution is to deploy detectors far from the ground to keep away from these noises.

Many GW space exploration plans have been proposed, among which LISA [7,8], TAIJI [9], and TianQin [10] are the most notable projects and have been under construction. All three missions have a similar structure consisting of a triangular array of three satellites. The detections of GW are accomplished by precisely measuring the changes in the arm length. TAIJI and LISA have similar orbits, and the angle between the plane formed by their own three satellites and the ecliptic plane is 60° so as to ensure the stability of the structure while the satellites are moving [11]. As a consequence, the normal vector of the detector plane will rotate around the normal vector of the ecliptic plane when TAIJI and LISA are operating [7–9]. In contrast, the TianQin mission is distinguished by its configuration of three identical drag-free satellites, which orbit the Earth in a nearly equilateral triangular constellation. Each satellite follows a Keplerian orbit with a period of approximately 3.65 days, primarily influenced by the gravitational attraction from the Earth. The guiding center of the constellation aligns with the geocenter and orbits the Sun along the ecliptic path. Notably, the detector plane's normal vector is directed toward the tentative reference source RX J0806.3 + 1527 [10,12].

The successful detection of GWs has unlocked a new field to understand the Universe. In fundamental physics, we can test the mass of gravitation, the polarizations, and the speed of GWs [13,14], etc. A number of questions, like the forming mechanism of the supernova [15,16], the progenitor of the short gamma-ray burst [17,18], the equation of the state of the neutron star [19,20], the more accurate measurement of the Hubble's constant, and so on [21,22], may be addressed through multimessenger observations combining GWs and electromagnetic signals. Tackling these science goals requires accurate measurements of GW parameters especially the source position.

*lmx@hust.edu.cn

 © 2023 American Physical Society

In reality, precise localization of GW sources is of paramount importance in facilitating multimessenger observations. It is only through the acquisition of accurate positional data that follow-up investigations into electromagnetic counterparts or the identification of the host galaxy can be rendered feasible.

Numerous studies have already addressed the issues of parameter estimation and localization accuracy for compact binary coalescence signals detected by ground-based detectors, encompassing different detector networks, GW templates of varying precision, and various parameter estimation methods [23–30]. Space-based detectors will target a wider range of GW signals compared to ground-based detectors, including not only coalescence signals from supermassive black hole binaries but also early inspiral signals from smaller mass compact star systems. Moreover, the orbital motion-induced signal amplitude and frequency modulation will result in distinct parameter estimation for space-based detectors compared to ground-based ones. It is noteworthy that Michelson interferometers are predominantly used in ground-based detectors, where the equal length of their two arms can effectively eliminate laser frequency noise. Unlike ground-based detectors, space-based detectors face challenges due to their relatively long arm lengths in comparison to the laser divergence, which hinders proper interferometry. Additionally, the inherent variability in the arm lengths of space-based detectors makes it impractical to eliminate laser frequency noise by directly combining the output signals. To address this dominant source of noise in space-based detectors, time-delay interferometry (TDI) techniques have been employed [31–33]. The objective is to mitigate laser frequency noise by means of a linear combination of multiple suitably delayed data streams and generate an output signal with minimal laser frequency noise.

The first attempt to estimate the sky position of binary black holes and monochromatic sources with LISA was made by Peterseim *et al.* [34–36]. The following more detailed studies are shown in Refs. [37–41], which include more accurate wave forms and more realistic detector response. The precision of the angular resolution of coalescing massive black holes and monochromatic sources with the LISA-TAIJI network was discussed in Refs. [42–44], whose conclusion is that the LISA-TAIJI network can improve the localization accuracy by 1–2 orders of magnitude compared with that of each individual detector. Those articles [45,46] investigate the accuracy of parameter estimation of supermassive black hole binary inspirals and Galactic double white dwarf binaries for TianQin and the TianQin-LISA network. Zhang [47,48] analyzed the dependence of monochromatic sources' parameter estimation errors on frequency and direction for LISA and TianQin. The parameter estimation and localization analysis of ringdown and inspiral signals containing higher order modes utilizing various space detector networks was discussed in Refs. [49,50]. Marsat *et al.* [51] utilized Bayesian analysis to examine the level of parameter estimation for complete inspiral-merger-ringdown (IMR) signals by LISA, and identified that higher-order modes can effectively break degeneracies between parameters.

Owing to the geometry and TDI data characteristics intrinsic to space-based detectors, each individual detector inherently constitutes a networked array.[1] Such built-in multichannel configurations can enhance parameter estimation capabilities at negligible additional cost. However, the full benefits of the networked design cannot be realized in the event of one arm failure. It is imperative to evaluate the resultant impact on parameter estimation performance. We will delineate the disparities in parameter estimation potential among various TDI channels, analyzing monochromatic sources and coalescing supermassive black hole (SMBH) binaries separately. Furthermore, we will quantify the enhancements in parameter estimation accuracy conferred by utilizing multichannel data relative to single channel. Moreover, for the coalescence of SMBH binaries, we will consider IMR signals incorporating higher-order modes. This represents the first application of IMR signals with higher modes on TianQin. We will contrast the parameter estimation accuracy achieved using single-channel signals with higher modes versus multichannel signals restricted to the dominant mode alone. This comparison will elucidate the relative contributions of higher modes and multiple channels to improving measurements of SMBH binary parameters.

The paper is structured as follows. In Sec. II, we provide a review of TDI combinations and the method for parameter estimation. Detailed information about the orbits for detectors is presented in the Appendix. In Sec. III, we investigate the parameter estimation error with various data combinations for monochromatic sources, while in Sec. IV, we examine the same for coalescing SMBH binaries. We summarize and discuss our findings in Sec. V.

II. METHODOLOGY

A. TDI and the response to GW

In this work, we use two reference frames. One is called the GW coordinate $\{\mathbf{e}_x, \mathbf{e}_y, \mathbf{e}_z\}$, in which the $\mathbf{e}_z$ axis stands for the propagation direction of GW. The other one is the observer's coordinate $\{\mathbf{i}, \mathbf{j}, \mathbf{k}\}$. Setting up the Solar System barycentric (SSB) coordinate system is a very convenient choice, considering the orbital motion of the satellites. The unit vectors $\{\mathbf{e}_x, \mathbf{e}_y, \mathbf{e}_z\}$ can be expressed as

[1]In practice, a network of different channels on the same detector often experiences noise-related issues, which sets it apart from a physically separate detector network (with independent noises). However, for the purpose of our analysis, we have chosen to simplify this complex problem by assuming that the different TDI channels exhibit independent noise characteristics.

$$\begin{pmatrix}\mathbf{e}_x\\ \mathbf{e}_y\\ \mathbf{e}_z\end{pmatrix}=\begin{pmatrix}\cos\phi\cos\theta\cos\psi-\sin\phi\sin\psi & \sin\phi\cos\theta\cos\psi+\cos\phi\sin\psi & -\sin\theta\cos\psi\\ -\cos\phi\cos\theta\sin\psi-\sin\phi\cos\psi & \cos\phi\cos\psi-\sin\phi\cos\theta\sin\psi & \sin\theta\sin\psi\\ -\cos\phi\sin\theta & -\sin\phi\sin\theta & -\cos\theta\end{pmatrix}\begin{pmatrix}\mathbf{i}\\ \mathbf{j}\\ \mathbf{k}\end{pmatrix}, \tag{1}$$

where θ and ϕ denote the angular coordinates of the source relative to the SSB coordinate, and ψ represents the polarization angle of the GW. The GW signals can be described as

$$H=\sum_{p=+,\times}\mathbf{e}^p h_p, \tag{2}$$

with

$$\begin{aligned}\mathbf{e}^+&=(\mathbf{e}_x\otimes\mathbf{e}_x-\mathbf{e}_y\otimes\mathbf{e}_y)/2,\\ \mathbf{e}^\times&=(\mathbf{e}_x\otimes\mathbf{e}_y+\mathbf{e}_y\otimes\mathbf{e}_x)/2.\end{aligned} \tag{3}$$

For the early inspiral signals of compact binary stars, considering them as monochromatic sources is appropriate due to the evolution timescale of their frequency being much longer than the operational lifespan of the detectors. So we have

$$\begin{aligned}h_+&=\mathcal{A}[1+\cos^2\iota]\exp(2\pi ift+i\phi_0),\\ h_\times&=2i\mathcal{A}\cos\iota\exp(2\pi ift+i\phi_0).\end{aligned} \tag{4}$$

And the amplitude parameter $\mathcal{A}$ is expressed as $\mathcal{A}=\frac{4(G\mathcal{M}_c)^{5/3}}{c^4D_L}(\frac{2\pi f}{2})^{2/3}$, where ι is the inclination angle between the GW and the orbital angular momentum of the binaries, f is the frequency of GW, ϕ_0 is the initial phase, D_L is the luminosity distance of the GW source, and $\mathcal{M}_c=m_1^{3/5}m_2^{3/5}/(m_1+m_2)^{1/5}$ is the chirp mass.

The principle of TDI is to eliminate laser frequency noise by linear combination of multiple appropriately delayed outputs, which gives $S=\sum_{j,k}d_{jk}s_{jk}$, where s_{jk} is the output measured at spacecraft k with transmission from spacecraft j, and d_{jk} is the time delay operator acting on the output s_{jk}. Then we can write [52]

$$s_{jk}=(\mathbf{n}_{jk}(t)\otimes\mathbf{n}_{jk}(t)):(HL_{jk}(t)/L_e)\mathcal{T}(f,t), \tag{5}$$

with

$$\begin{aligned}\mathcal{T}(f,t)=&\sin c[\omega L_{jk}(1-\mathbf{e}_z\cdot\mathbf{n}_{jk})/2]\\ &\times\exp[-i\omega(L_{jk}+\mathbf{e}_z\cdot\mathbf{X}_k+\mathbf{e}_z\cdot\mathbf{X}_j)/2],\end{aligned} \tag{6}$$

where $\omega=2\pi f$, L_{jk} is the arm length between spacecraft j and spacecraft k, L_e is the expected arm length, $\mathbf{n}_{jk}$ is the unit vector from spacecraft j to spacecraft k, and $\mathbf{X}_j$ is the location of spacecraft j.

For GW from coalescing supermassive black holes binaries, the frequency-domain polarization is

$$\begin{aligned}h_+(f)&=\sum_{l,m}\frac{1}{2}({}_{-2}Y_{lm}+(-1)^l{}_{-2}Y^*_{l,-m})h_{lm}(f),\\ h_\times(f)&=\sum_{l,m}\frac{i}{2}({}_{-2}Y_{lm}-(-1)^l{}_{-2}Y^*_{l,-m})h_{lm}(f),\end{aligned} \tag{7}$$

where ${}_{-2}Y_{lm}$ are the spherical harmonics of spin-weight -2 [53]. $l\geq 2$ and $-l\leq m\leq l$ are known as the harmonic indices. And $h_{lm}=A_{lm}(f)e^{-i\Phi_{lm}(f)}$ are the spherical harmonics. The dominant harmonic is h_{22}, while the remaining ones are referred to as higher-order modes. In this work, we will use the IMRPhenomXHM model, which includes higher-order modes, to generate the full IMR signals [54]. The LALSuite and PyCBC are employed for the implementation of the numerical waveform [55,56]. While the dominant harmonic is typically sufficient for comparable-mass binaries or weak signals, incorporating higher-order modes becomes crucial for binaries with unequal masses or stronger signals, as is often encountered in space-based GW detection [57–59]. In order to simplify the calculation, we will focus on the four most prominent modes in this analysis:

$$(l,m)=(2,2),(2,1),(3,3),(4,4). \tag{8}$$

Owing to the distinct frequency and phase evolution of various modes, employing mode-by-mode single-link response is a practical approach,

$$s^{lm}_{jk}=(\mathbf{n}_{jk}(t_{lm})\otimes\mathbf{n}_{jk}(t_{lm})):(HL_{jk}(t_{lm})/L_e)\mathcal{T}(f,t_{lm}), \tag{9}$$

where

$$t_{lm}=-\frac{1}{2\pi}\frac{d\Phi_{lm}}{df} \tag{10}$$

is the effective time-frequency correspondence for each harmonic, determined from the stationary-phase approximation (SPA). Subsequently, the full output for various TDI combinations is

$$S=\sum_{j,k}\sum_{l,m}d_{jk}s^{lm}_{jk}. \tag{11}$$

While several generations of TDI techniques have been developed to address issues arising from the nonrigid

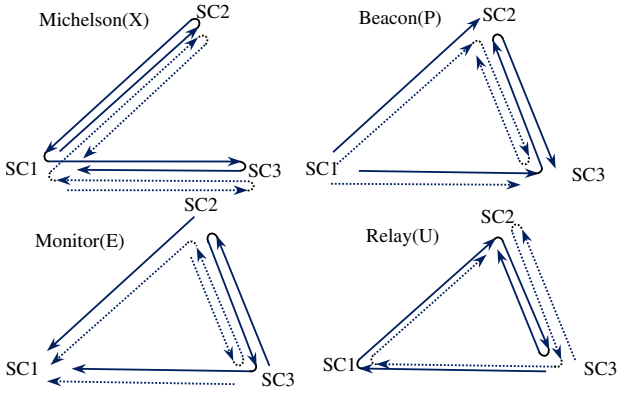

FIG. 1. The diagram of selected first generation TDI channels [unequal-arm Michelson (X), Monitors (E), Beacons (P), and Relays (U)].

motion and rotational dynamics of spacecraft within a GW detector array, the refinements introduced in higher-generation TDI solutions provide only minimal influence in response to GW signals [60–62]. In this research, we concentrate on the four-link configurations of first generation TDI combinations, which include unequal-arm Michelson (X, Y, Z), Beacons (P, Q, R), Monitors (E, F, G), and Relays (U, V, W). The first channels of these combinations are shown in Fig. 1, and others can be determined by cyclical permutation of the spacecraft indices. Another approach to TDI channels, called noise-orthogonal channels, obtains channels through linear combinations of the known elements of TDI channels. These noise-orthogonal channels are independent under the assumption of an identical and uncorrelated noise in the detector arms. This noise-orthogonalization technique aims to minimize the contamination of gravitational wave signals by laser frequency noise and other instrumental errors [33,63]. Here we choose to compose the optimal TDI channels using the unequal-arm Michelson (X, Y, Z) [64],

$$A_X = \frac{Z-X}{\sqrt{2}}, \quad E_X = \frac{X-2Y+Z}{\sqrt{6}}, \quad T_X = \frac{X+Y+Z}{\sqrt{3}} \tag{12}$$

B. Noise power spectral density

For space detectors, the dominant noise sources are acceleration noise and optical path noise, since the laser frequency noise has been eliminated by TDI combinations. For LISA, the single-link optical path noise is [65]

$$P_{\mathrm{op,LISA}} = (1.5 \times 10^{-11}\ \mathrm{m})^2 \left[1 + \left(\frac{2\ \mathrm{mHz}}{f}\right)^4\right] \mathrm{Hz}^{-1}, \tag{13}$$

and the acceleration noise is

$$P_{\mathrm{ac,LISA}} = (3 \times 10^{-15}\ \mathrm{ms}^{-2})^2 \left[1 + \left(\frac{0.4\ \mathrm{mHz}}{f}\right)^2\right] \times \left[1 + \left(\frac{f}{8\ \mathrm{mHz}}\right)^4\right] \mathrm{Hz}^{-1}, \tag{14}$$

while for TianQin, the optical path noise is $P_{\mathrm{op,TQ}} = 10^{-24}\ \mathrm{m^2\,Hz^{-1}}$, and the acceleration noise is $P_{\mathrm{ac,TQ}} = 10^{-30}\ \mathrm{m^2\,s^{-4}\,Hz^{-1}}$ [10].

The equivalent optical path noise and equivalent acceleration noise can be obtained by

$$S_{\mathrm{op}} = P_{\mathrm{op}}/L^2, \qquad S_{\mathrm{acc}} = P_{\mathrm{acc}}/(\omega^2 L)^2. \tag{15}$$

Then the total noise power spectral density (PSD) functions of the selected TDI combinations are [32]

$$\begin{aligned}
S_X &= 16\sin^2 2x S_{\mathrm{op}} + 16(3+\cos 4x)\sin^2 2x S_{\mathrm{acc}},\\
S_P &= S_E = 8(3+2\cos 2x)\sin^2 x S_{\mathrm{op}}\\
&\quad + 16(3+\cos 2x)\sin^2 x S_{\mathrm{acc}},\\
S_U &= 8(4+4\cos 2x+\cos 4x)\sin^2 x S_{\mathrm{op}}\\
&\quad + 16(5+5\cos 2x+2\cos 4x)\sin^2 x S_{\mathrm{acc}},\\
S_{A_X} &= S_{E_X} = 8(2+\cos 2x)\sin^2 2x S_{\mathrm{op}}\\
&\quad + 16(3+2\cos 2x+\cos 4x)\sin^2 2x S_{\mathrm{acc}},
\end{aligned} \tag{16}$$

where $x = \pi f L$. It is worth noting that the PSD equations presented above were derived under the assumption of $L1 = L2 = L3 = L$. This assumption is generally applicable to most data channels. However, taking into account the actual orbital motion, significant deviations in the noise power spectrum of the T channel are expected in the low-frequency domain compared to those obtained under this assumption [44]. In this study, we shall consider the time-varying evolution of T-channel noise.

C. Fisher information matrix method

The GW signals depend on a set of unknown parameters. To know the accuracy of the parameter estimation, one simple but powerful method called Fisher information matrix (FIM) has been widely employed [23,66]. Here we briefly introduce FIM as

$$\Gamma_{\alpha\beta} = \left(\frac{\partial S}{\partial \xi_\alpha}\middle|\frac{\partial S}{\partial \xi_\beta}\right), \tag{17}$$

where the $(A|B)$ denotes the inner product of A and B:

$$(A|B) = 4\Re \int_0^{+\infty} \frac{A(f)B^*(f)}{S_n(f)}\, df. \tag{18}$$

And for monochromatic GW sources, we can write

$$(A|B) = \frac{2}{S_n(f)} \Re \int_0^{T_0} A(t)B^*(t)dt, \tag{19}$$

where T_0 is the observation time, which is fixed to one year in all simulations in this work. With the definition of inner product above, the signal-to-noise ratio (SNR) ρ can be represented as $\sqrt{(S|S)}$. According to the Cramér-Rao inequality, the inverse FIM $\Gamma^{-1}_{\alpha\beta}$ is the lower bound for the error covariance of any unbiased estimator of the parameters. In the limit of significant SNR, the maximum likelihood estimator can be seen as unbiased, and $\Gamma^{-1}_{\alpha\beta}$ will be a good approximation for the covariance matrix [66], so the covariance matrix of the parameters is

$$\sigma_{\alpha\beta} \approx \Gamma^{-1}_{\alpha\beta}. \tag{20}$$

The standard deviations of the parameters are given by

$$\sigma_\alpha \approx \sqrt{\Gamma^{-1}_{\alpha\alpha}}. \tag{21}$$

The angular uncertainty of the sky localization is evaluated by [67]

$$\Delta_\Omega = 2\pi \sin\theta \sqrt{\sigma_{\theta\theta}\sigma_{\phi\phi} - \sigma^2_{\theta\phi}}. \tag{22}$$

And to demonstrate the enhanced positioning accuracy of multichannel in comparison to single channel, we introduce a novel metric,

$$r_\Omega = \frac{\Delta_\Omega \text{ with single channel}}{\Delta_\Omega \text{ with multiple channel}}. \tag{23}$$

Here we will also introduce the normalized FIM, which is commonly utilized in the analysis of monochromatic sources [68],

$$\tilde{\Gamma} = \frac{\Gamma}{\rho^2}. \tag{24}$$

And then the normalized error can be represented as

$$\tilde{\sigma}_\alpha = \sigma_\alpha \cdot \rho, \qquad \tilde{\Delta}_\Omega = \Delta_\Omega \cdot \rho^2. \tag{25}$$

D. Simulated GW sources

In this study, our primary focus is on the temporal and spectral dependencies of parameter estimation accuracy. To mitigate the impact of fluctuations in other parameters, we will randomly generate a broad range of samples and calculate the median errors across these samples. In the case of monochromatic sources, we investigate error propagation with respect to seven parameters $\{\theta, \phi, \psi, \log \mathcal{A}, \iota, f, \phi_0\}$, as

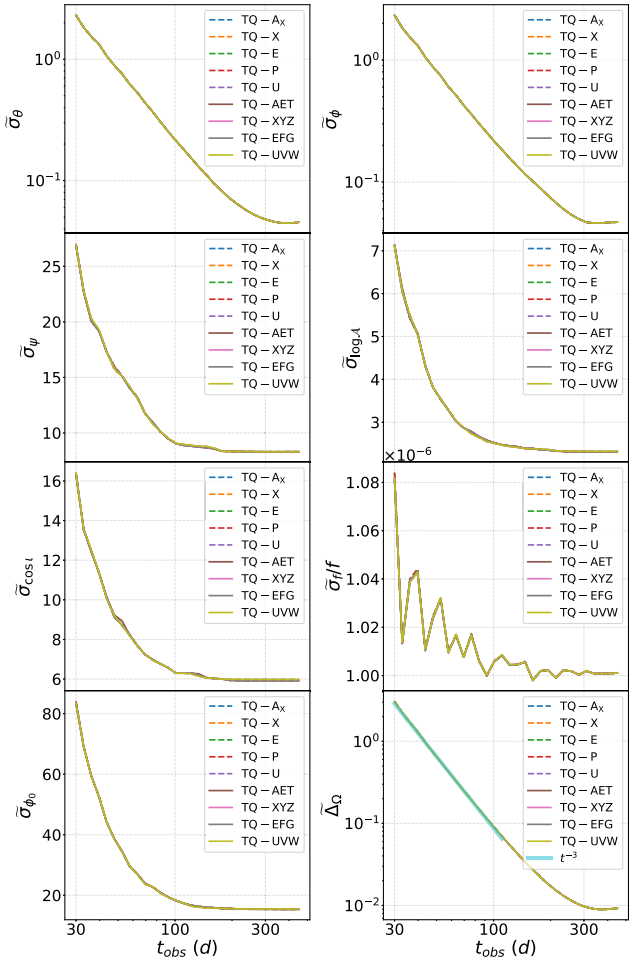

FIG. 2. The temporal dependence of the normalized parameter estimation errors with various data combinations for TianQin. The dashed lines depict the normalized parameter errors obtained from single-channel data, while the solid lines represent those derived from multichannel data.

defined in detail in Sec. II A. We simulate 1000 sources with the parameters $\theta, \phi, \psi, \cos\iota$, and ϕ_0 uniformly distributed within their corresponding domain of definition, and assess the accuracy of parameter estimation for these samples based on a specific detection time and frequency.

For coalescing SMBH binaries, we consider the error evolution of eight parameters, namely sky-position parameters $\{\theta, \phi\}$ defined in the SSB coordinate system (similar to the monochromatic Scenario), GW polarization angle ψ, the source-frame total mass $M_{\rm tot}$, mass ratio q, luminosity distance D_L, inclination ι, and coalescence phase ϕ_c. The total mass range studied in this research includes $\{8\times10^4, 2\times10^5, 4\times10^5, 8\times10^5, 2\times10^6, 4\times10^6, 8\times10^6, 2\times10^7, 4\times10^7 M_\odot\}$. All systems have a fixed representative mass ratio of $q = 3$ and are located at the same redshift of $z = 1$.[2]

[2]We employ the Planck18 Cosmological parameters to facilitate the conversion between luminosity distances and redshifts [69].

We generate 1000 samples with the parameters $\theta, \phi, \psi, \iota$, and ϕ_c uniformly distributed across their respective domains, and evaluate the accuracy of parameter estimation for these samples at a specific mass and detection time.

III. PARAMETER ESTIMATION FOR MONOCHROMATIC GW SOURCES

In this section, we investigate how the temporal and spectral characteristics affect the accuracy of parameter estimation for monochromatic sources. In the calculation, we consider a range of single TDI channels and multichannel networks for both TianQin and LISA.

A. Time dependence

Considering the impact of the detector's orbital motion on amplitude and phase modulation, significant improvements in parameter estimation accuracy are anticipated within one year of observation. However, detecting monochromatic sources in less than one month may not be feasible. Therefore, we will investigate the progression of parameter error in detection time over a span of one to fifteen months at a frequency of 10 mHz. We have considered various data combinations in this calculation. To present the results concisely, we will utilize the normalized accuracies. The medians of the normalized parameter estimation errors are presented in Fig. 2 for TianQin and Fig. 3 for LISA.

For TianQin, all data combinations exhibit the same trend in the evolution of normalized parameter errors. When the observation time exceeds 3.65 days, amplitude modulation no longer impacts parameter error evolution due to the fixed direction and rotation period of the detector plane. The benefits of multichannel networking are then solely dependent on SNR improvements. Furthermore, when the observation period is less than one year, the Doppler effect dominates the evolution of the normalized parameter error. The positional parameter errors undergo significant evolution, and during the initial stage, the localization error can be characterized by a power law with an index of -3.

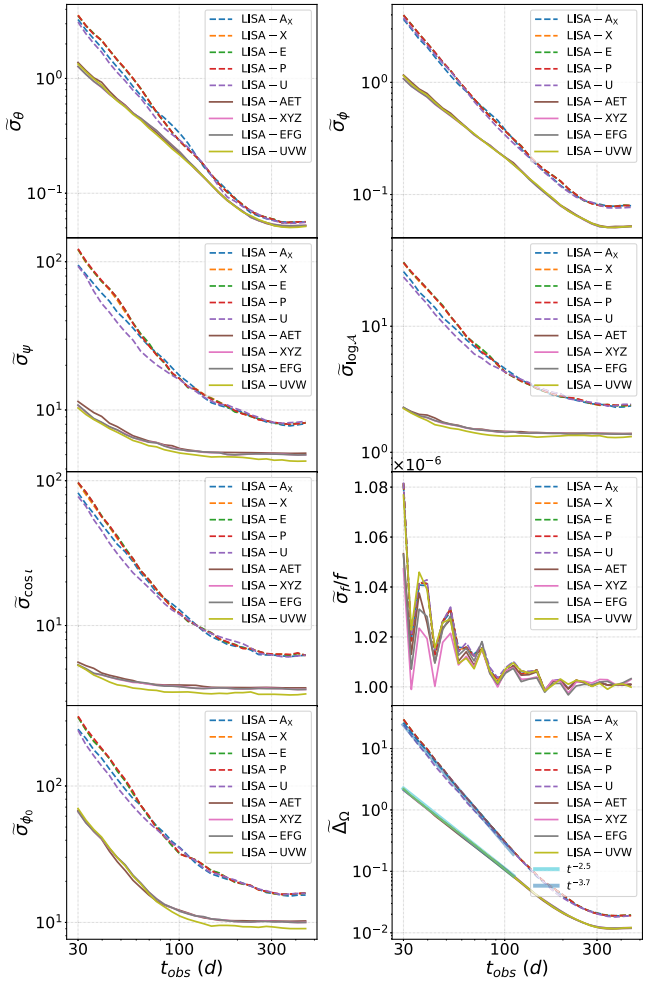

FIG. 3. The same as Fig. 2 but for LISA.

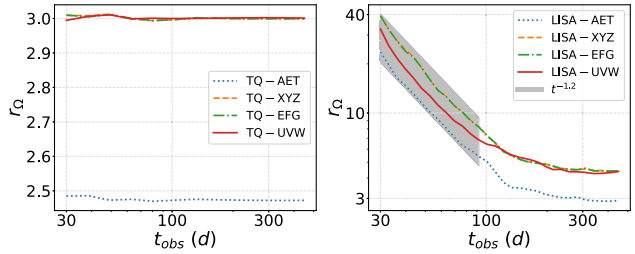

FIG. 4. The improvement of localization accuracy as a function of time for TianQin (left panel) and LISA (right panel). r_Ω stands for the ratio between the localization accuracy with single-channel data and that with multichannel data.

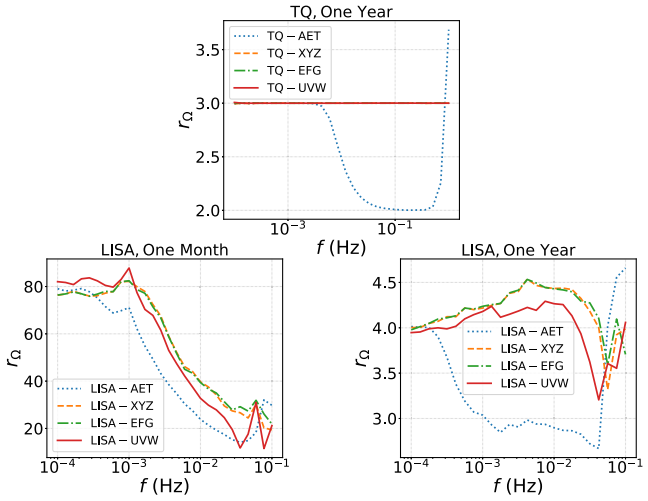

FIG. 5. The improvement of localization accuracy as a function of frequency for TianQin (upper panel) and LISA (lower right panel) with a one-year observation, as well as for LISA (lower left panel) with a one-month observation. r_Ω stands for the ratio between the localization accuracy with single-channel data and that with multichannel data.

For LISA, multichannel networks show significant improvement in parameter accuracy except frequency compared to single channels. However, the degree of improvement decreases with increasing observation time. Secondly, due to the constantly changing orientation of the LISA detector plane, even with a cumulative detection time exceeding one year, there remains a discrepancy between a single-channel and multichannel network on the normalized accuracies. Finally, the time evolution of the normalized parameter error is primarily influenced by the combined effects of Doppler shift and antenna pattern modulation. And in the initial stages, the positioning errors of a single-channel and multichannel network can be described by power laws with indexes of -3.7 and -2.5, respectively.

The enhancement of localization accuracy with multichannel data in contrast to that with single-channel data is demonstrated in Fig. 4. For TianQin, the multichannel network XYZ, UVW, and EFG can improve localization accuracy by approximately twice that of the single channel X, U, and E. However, the optimal multichannel network AET exhibits a slightly weaker improvement due to the low SNR of its T channel at 10 mHz. The localization accuracy improvement achieved by the multichannel network for LISA showcases a diminishing trend over time, from an initial improvement of more than 1 order of magnitude in one month to 3 to 4 times after one year. The power law with an index of -1.2 in the figure is derived from the two power laws depicted in Fig. 3. It is noteworthy that the time-varying nature of the detector plane's normal vector enables LISA's multichannel network to yield greater improvements on various parameter errors than TianQin, even after a year has elapsed.

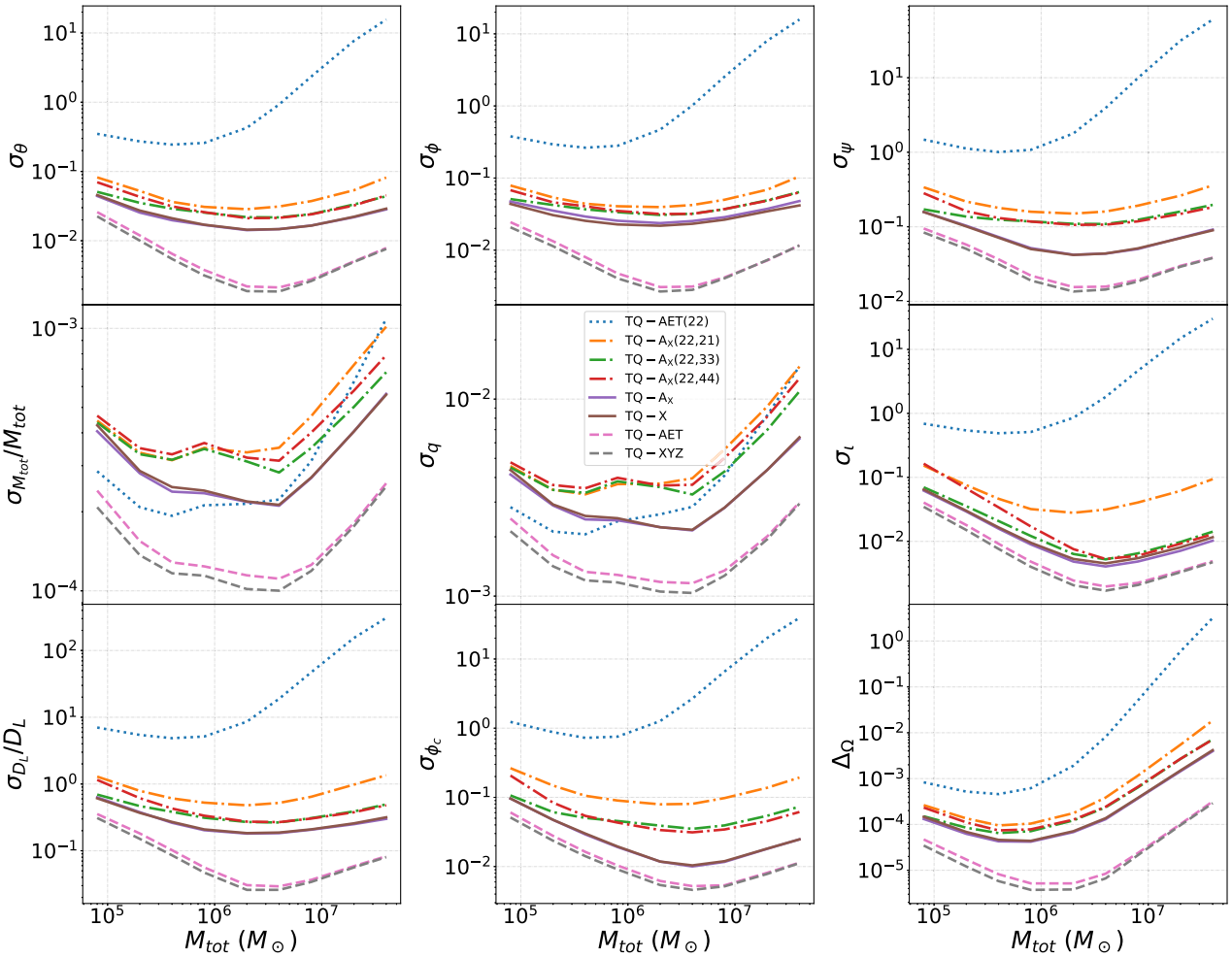

FIG. 6. The evolution of the parameter estimation accuracies as functions of mass for coalescing SMBH binaries by TianQin under various scenarios. The dotted line denotes the results from multichannel data using only the 22-mode signal. The dot-dashed line represents the results from single-channel data using the 22-mode plus one higher-order mode signal. The solid line shows the single-channel results with all mode signals, and the dashed line corresponds to the multichannel results with all mode signals included.

B. Frequency dependence

The parameter estimation based on Michelson-type data as a function of frequency has been studied in Ref. [48] with detailed analysis. Under the low-frequency approximation condition, it can be easily demonstrated that the normalized parameter error is independent of the choice of data combinations. Therefore, we place greater emphasis on the correlation between the enhancement of localization accuracy resulting from multichannel networks across different detectors and their corresponding frequencies, as illustrated in Fig. 5. When the detection time exceeds one year, there is no apparent frequency dependence in the improvement of localization accuracy brought by TianQin's and LISA's multichannel networks. The difference between AET and other multichannel networks mainly lies in the middle and high frequencies. For a detection time of one month, the localization accuracy improvement provided by LISA's multichannel networks exhibits significant frequency dependence. There is an order of magnitude decrease in accuracy from low to high frequencies due to the increasing dominance of the Doppler effect on localization.

IV. PARAMETER ESTIMATION FOR COALESCING SMBH BINARIES

Unlike the relatively slow frequency evolution of early inspiral signals, the coalescence of the SMBH binary represents the most dramatically evolving GW signal that can be detected by space missions. In this section, we will examine the parameter estimation accuracies of TianQin and LISA for such signals. We utilize the complete IMR signal spanning from 30 days prior to coalescence until the ringdown phase. In the calculation, we consider various scenarios, including a multichannel network consisting only of the 22 mode, a single-channel with both the 22 mode and a higher mode, a single-channel incorporating all modes, and finally a multichannel network encompassing all modes. Previous calculations indicate that different combinations of data yield similar levels of accuracy in

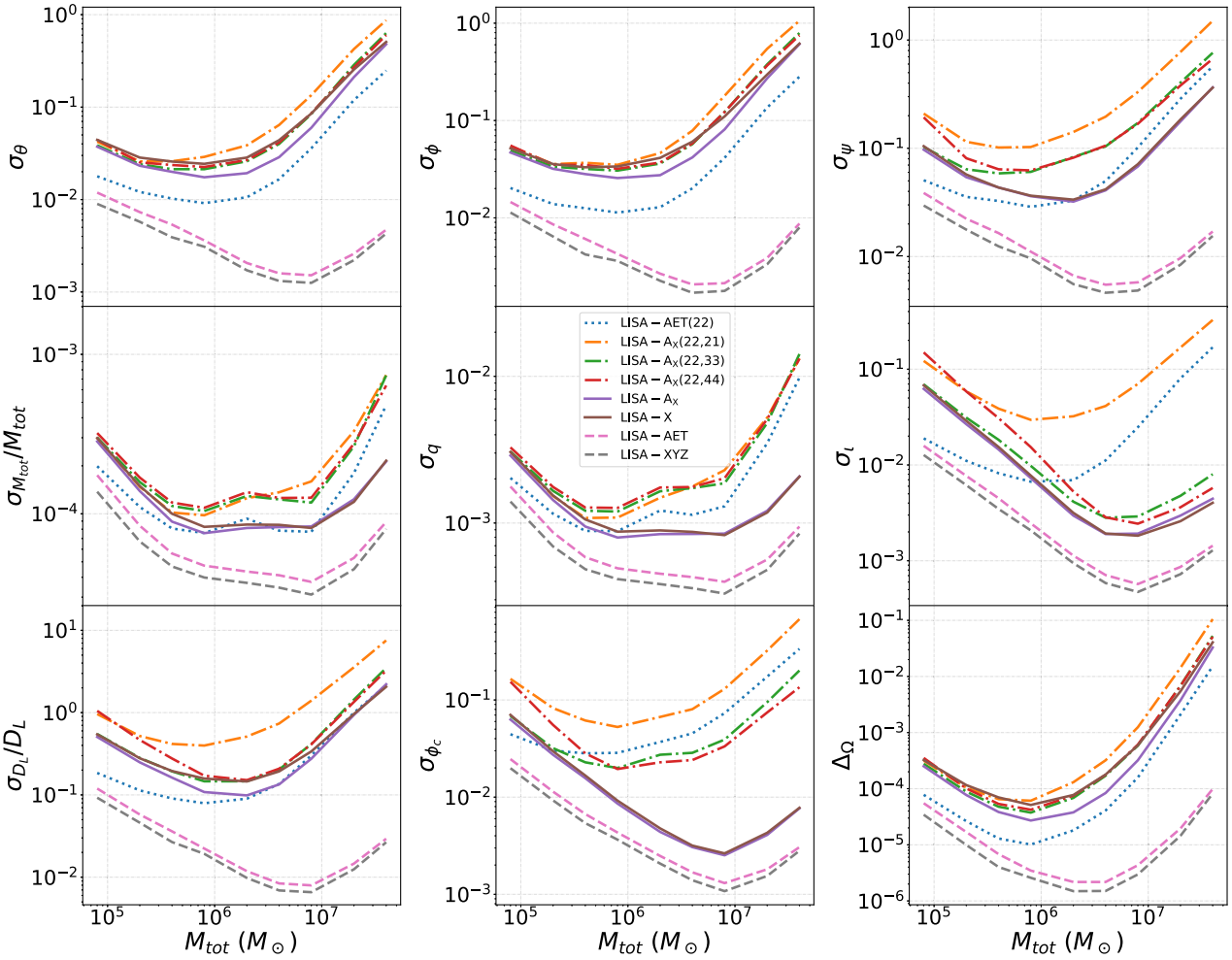

FIG. 7. The same as Fig. 6 but for LISA.

parameter estimation. To enhance conciseness, we will solely consider the XYZ and AET combinations in this section.

A. Mass dependence

We employ TianQin and LISA to infer the parameters of SMBH systems with varying total masses at a fixed redshift $z = 1$. The medians of parameter errors are presented in Fig. 6 for TianQin and Fig. 7 for LISA. From Figs. 6 and 7, one can find for most parameters except ι, the 22 mode plus any higher mode exhibit the comparable parameter estimation error. As a parameter in functions ${}_{-2}Y_{lm}$, the estimation accuracy of ι is more dependent on multimode detection. With increasing mass, the relative contribution of the 21 mode to the SNR diminishes, leading to a relatively suboptimal performance in the parameter estimation for ι.

Furthermore, there exist disparities between the results of TianQin and LISA. With regard to TianQin, apart from the parameters concerning $M_{\rm tot}$ and q, the parameter estimation error associated with multichannel network detection of the 22 mode is comparatively weaker than that of multimode single-channel detection. Moreover, this discrepancy will magnify as the total mass increases. The enhancement in parameter estimation precision of multimode with multichannel network detection gradually diminishes beyond a total mass of $2 \times 10^6 M_\odot$, compared to that of multimode single-channel data. For LISA, the parameter estimation error of multichannel network detection in the 22 mode is comparable to that of single-channel detection in multimode. The improvement provided by a multimode multichannel network, compared to multimode single-channel data, increases with mass.

To comprehend the aforementioned disparities between TianQin and LISA, we conducted a computation of

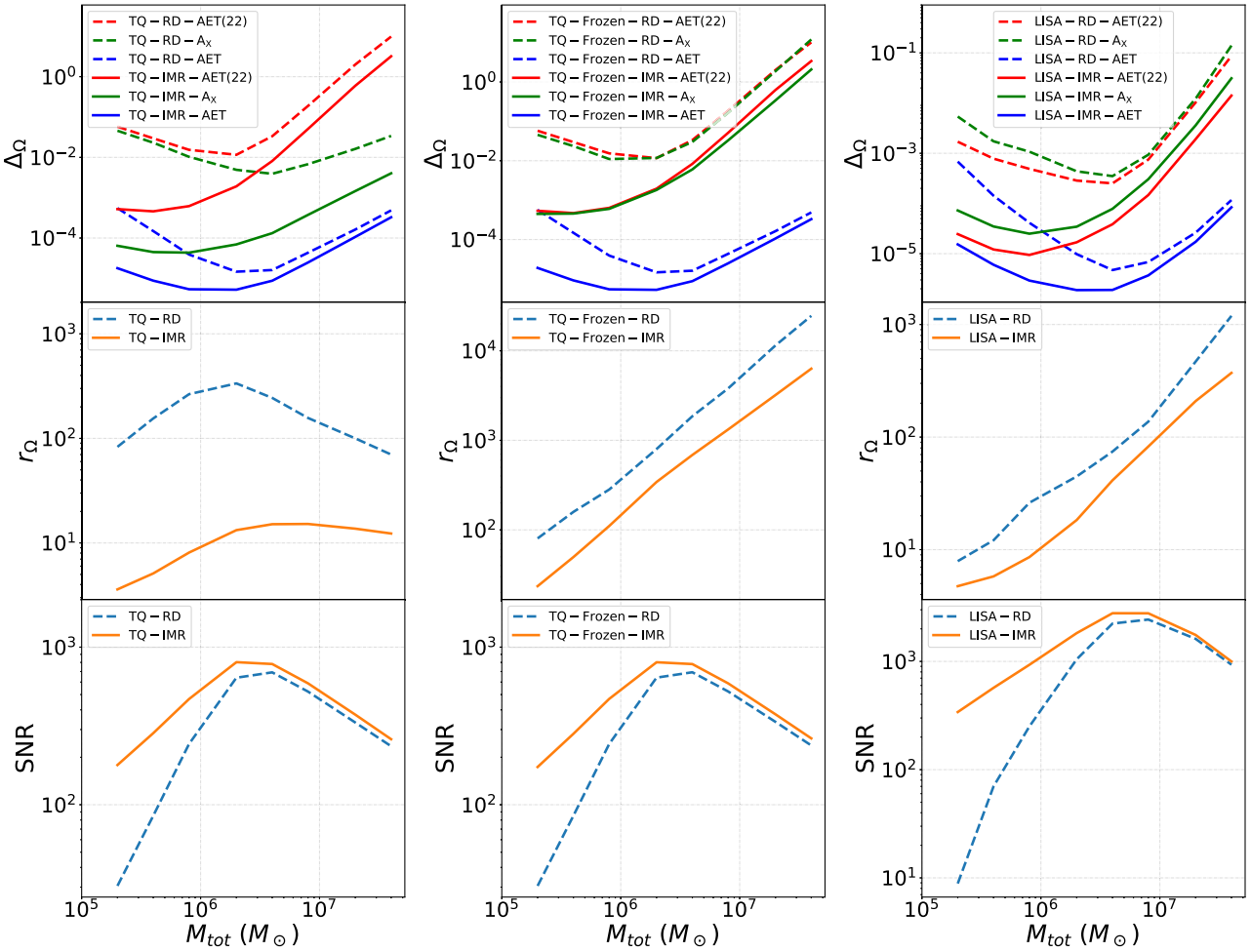

FIG. 8. The evolution of the localization accuracy of space-based detectors as a function of mass for ringdown signal and IMR signal under various scenarios. The dotted line denotes the results from ringdown signal, and the dashed line corresponds to the results with IMR signal. The left panels exhibit the localization accuracy, enhancement of multichannel localization precision relative to single-channel and SNR, which are attained by using TianQin under various circumstances, while the middle and right panels are the same as the left panels but for TianQin-Frozen and LISA, respectively.

localization accuracy evolution with respect to mass for both detectors during the ringdown stage and complete IMR waveform, as depicted in Fig. 8. Additionally, we incorporated a virtual detector named TianQin-Frozen that disregards antenna pattern modulation and Doppler effect caused by TianQin's orbital motion. For short-term and rapidly evolving burst signals, such as binary black hole mergers, there are primarily three factors that affect the localization with a single detector: (1) modulation of a single-channel or multichannel antenna pattern due to detector motion, (2) modulation due to frequency evolution of response function $\mathcal{T}$, and (3) different responses of the detector to different mode signals. Owing to the concentration of SNR in the ringdown and short-time signal prior to merging, the Doppler effect induced by detector movement does not impact the localization. It is important to note that the multichannel network of TianQin remains unaffected by antenna pattern modulation caused by detector movement, as the detector plane of the TianQin consistently faces a fixed direction.

Based on the results of TianQin and TianQin-Frozen, it can be inferred that for TianQin, when the total mass is below $2 \times 10^6 M_\odot$, the damping time of the ringdown stage is short (less than four minutes) and the antenna pattern modulation caused by detector movement can be neglected. Under such circumstances, both the 22-mode multichannel network detection and multimode single-channel detection exhibit similar localization performance. Furthermore, the premerger signal contributes to a higher SNR, resulting in significantly improved localization accuracy of the complete IMR signals compared to that of the signals containing only the ringdown stage. In the scenario where

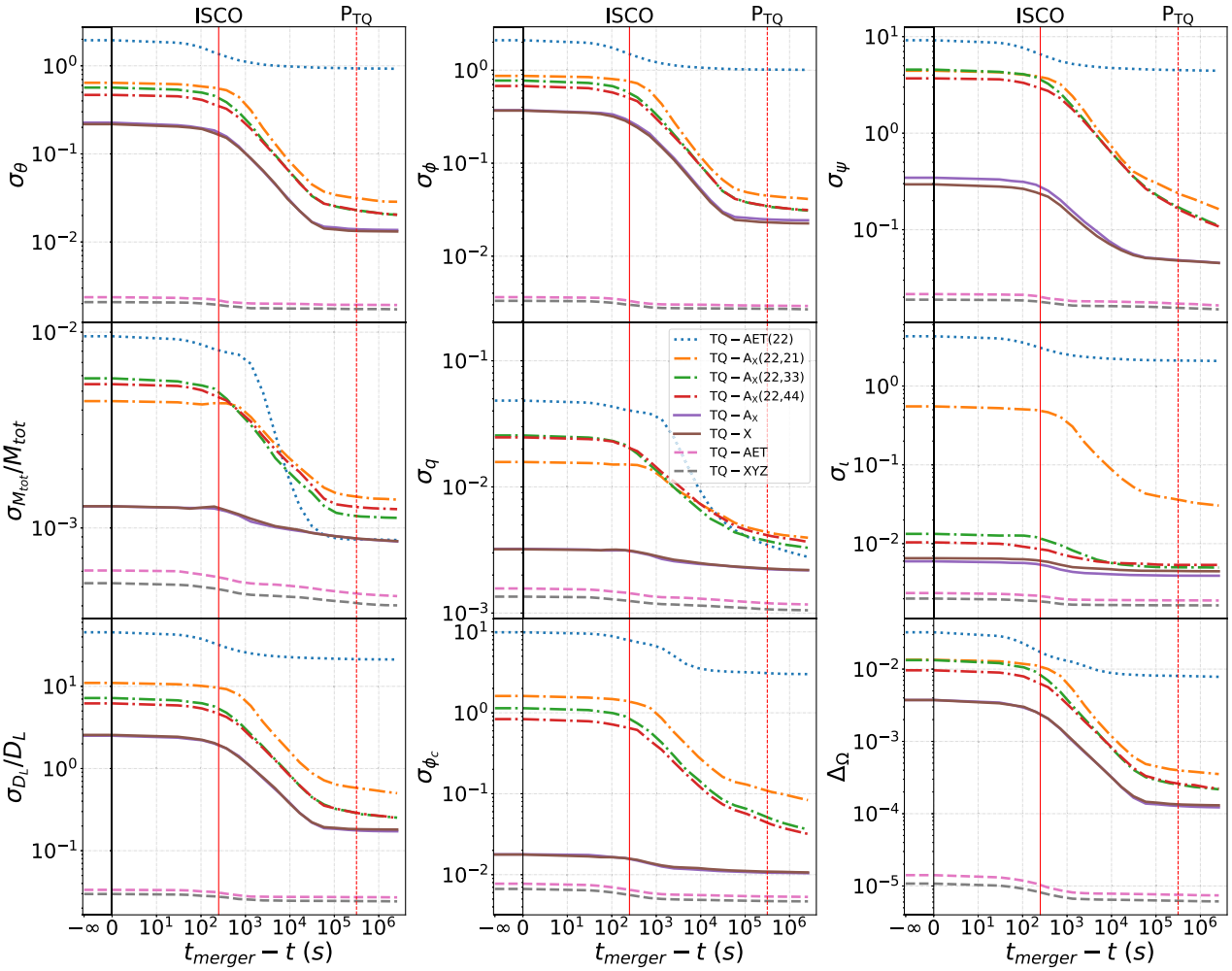

FIG. 9. The evolution of the parameter estimation accuracy as a function of time for coalescing SMBH binaries [with the mass of $(10^6, 3 \times 10^6) M_\odot$] by TianQin under various scenarios. The dotted line denotes the results from multichannel data using only the 22-mode signal. The dot-dashed line represents the results from single-channel data using the 22 mode plus one higher-order mode signal. The solid line shows the single-channel results with all mode signals, and the dashed line corresponds to the multichannel results with all mode signals included. The red descending solid line denotes the time corresponding to ISCO, while the red descending dashed line represents the detector plane rotation period (3.65 d) of TianQin.

$2 \times 10^6 M_\odot < M_{\rm tot} < 4 \times 10^7 M_\odot$, the damping time of the ringdown stage ranges from four minutes to over one hour. Notably, the implementation of antenna pattern modulation profoundly improves the localization accuracy of multimode single-channel data, surpassing that achieved by the 22-mode multichannel data. Simultaneously, the ringdown phase commences to dominate the SNR of the observation period, progressively reducing the disparity between the localization precision of the ringdown signal and that of the IMR signal. Regarding the enhancement brought by the multichannel network, it can be observed that when the total mass is small, the modulation of response function $\mathcal{T}$ dominates the localization accuracy. As total mass increases, the contribution of antenna pattern modulation becomes more pronounced, and r_Ω gradually increases. However, when the total mass exceeds $2 \times 10^6 M_\odot$, the detector rotation causes a gradual decline in r_Ω.

By comparing the localization accuracy of TianQin-Frozen and LISA, we can observe that for LISA, when only the ringdown signal is considered, the antenna pattern modulation caused by detector movement can be overlooked within the mass range of our interest. In this scenario, the 22-mode multichannel network and multimode single channel exhibit similar localization performance, with r_Ω gradually increasing as mass increases. When the complete IMR signal is considered, both the single-channel and multichannel network are affected by antenna mode modulation caused by the constantly changing detector plane normal vector of LISA. In this scenario, the localization performance of the 22-mode multichannel network and multimode single channel remains comparable, while r_Ω will also increase with mass.

B. Time dependence

In the preceding subsection, we investigated the localization of both ringdown and full IMR signals by TianQin and LISA in various scenarios. To comprehend these findings, it is beneficial to examine how all parameters evolve over time. Given the high SNR of the ringdown phase signal in SMBH mergers, we concentrate on the impact on errors of cumulative detection time prior to merging. We consider multiple systems with a total mass of

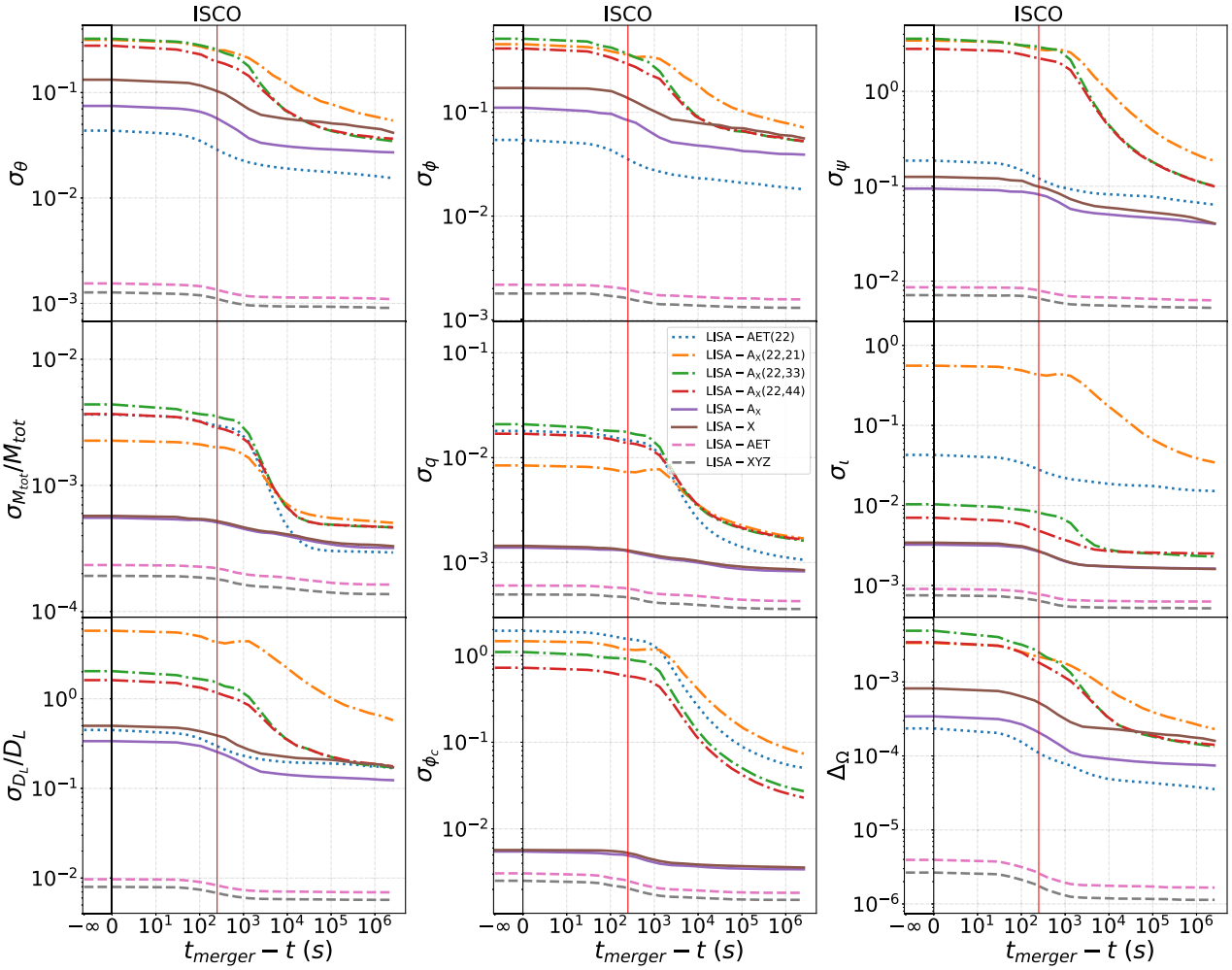

FIG. 10. The same as Fig. 9 but for LISA.

$4 \times 10^6 M_\odot$, where the SNR during the observation period is dominated by the ringdown phase, and the medians of parameter errors are shown in the Figs. 9 and 10 for the two missions.

For TianQin, it can be observed from Fig. 9 that the parameter constraints for multimode multichannel network detection remain constant over time, with only a slight variation at the time corresponding to the Schwarzschild innermost stable circular orbit (ISCO). Antenna pattern modulation has a significant impact on the error evolution of parameters like θ, ϕ, ψ, D_L, while single-channel data exhibit improvements in these parameters by 1 to 2 orders of magnitude over time. Moreover, the inclusion of additional higher-order modes has a significant impact on the accuracy of estimating the parameters like $M_{\rm tot}, q, \phi_c, \iota$ in the ringdown signal. However, as the phase accumulates, the influence of these higher-order modes will greatly diminish.

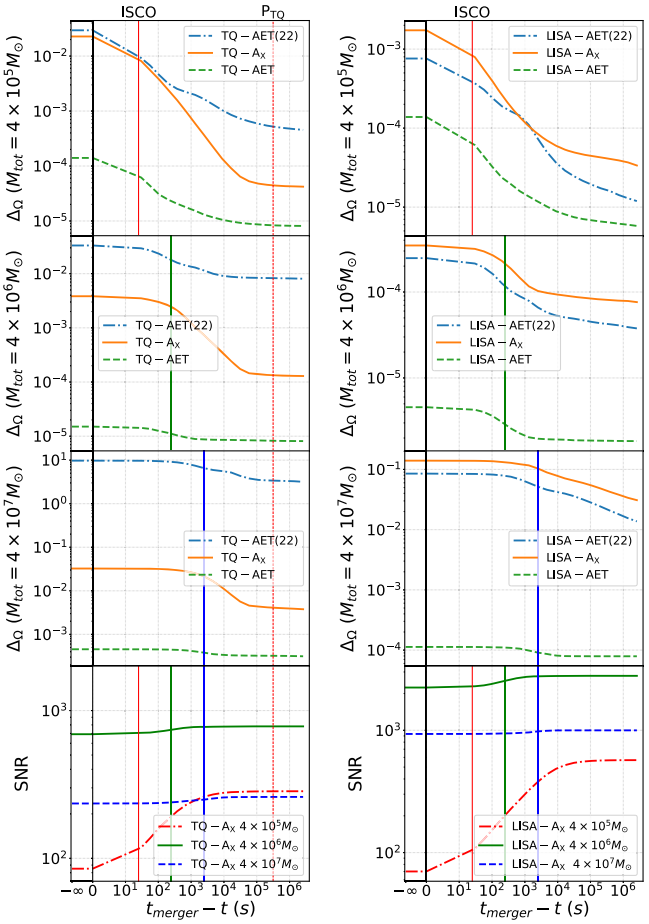

FIG. 11. The evolution of the localization accuracy of space-based detectors as a function of time for coalescing SMBH binaries under various scenarios. The left panel shows the localization accuracy and SNR attained by TianQin under various scenarios for binary black hole systems with masses of $(10^5, 3 \times 10^5) M_\odot$, $(10^6, 3 \times 10^6) M_\odot$, and $(10^7, 3 \times 10^7) M_\odot$ respectively. The descending solid lines in red, green, and blue represent the time corresponding to ISCO for SMBH binaries with masses of $(10^5, 3 \times 10^5) M_\odot$, $(10^6, 3 \times 10^6) M_\odot$, and $(10^7, 3 \times 10^7) M_\odot$ respectively, while the descending red dashed line denotes the detector plane rotation period (3.65 d) of TianQin. The right panels are the same as the left panels but for LISA.

The parameter estimation error evolution of LISA generally resembles that of TianQin, with two notable differences. Firstly, LISA's 22-mode multichannel network provides the same level of parameter estimation as the multimode single channel data except the parameter ι. Secondly, owing to the one-year antenna pattern modulation period of LISA, the relevant parameters exhibit less temporal evolution compared to TianQin within the time range we are concerned with.

To examine the evolution of localization accuracy over time, we evaluate the localization precision corresponding to systems with total masses of $4 \times 10^5 M_\odot$ and $4 \times 10^7 M_\odot$ respectively for comparison. The corresponding medians of localization accuracy are depicted in Fig. 11. For binary black hole systems with a total mass of $4 \times 10^5 M_\odot$, it is evident that inspiral signals significantly impact localization. Taking the example of 22-mode multichannel data, TianQin and LISA present enhancements in magnitude by 3 and 2 orders respectively. As the total mass increases, SNR contributed by the inspiral signals decreases progressively, while the damping time of the ringdown signals extends. This implies that the inspiral phase becomes less informative for accurately determining the source location as the total mass of the binary system increases. For binary black hole systems with a total mass of $4 \times 10^7 M_\odot$, the multimode single channel data from both TianQin and LISA missions can yield improvements in localization accuracy by only approximately 1 order of magnitude during the inspiral phase.

V. CONCLUSIONS

In this study, we employ the FIM method to investigate the level of parameter estimation for space-based detectors in detecting monochromatic sources and coalescing SMBH binaries under various TDI combinations. For monochromatic sources, we analyze the evolution of normalized parameter estimation errors over a period ranging from 1 to 15 months. The results indicate that for TianQin, the trend in the evolution of single-channel data is consistent with that of multichannel data, and location-related parameters exhibit significant evolutionary trends. In the case of LISA, multichannel data present a remarkable enhancement in parameters with the exception of frequency, when compared to single-channel data. We also examine the temporal and spectral evolution of localization enhancement in multichannel networks relative to single-channel data. For TianQin, the improvement in localization achieved through multichannel processing reveals no discernible variation over time or frequency, maintaining a double

improvement. For LISA, the improvements in localization brought by multichannel networks demonstrate distinct temporal and spectral evolution characteristics when the detection time is less than one year, while it stabilizes at 3 to 4 times when the detection time exceeds one year.

Compared to monochromatic sources, the space-based detector offers much more comprehensive parameter estimation rules for coalescing SMBH binaries. We examine the evolution of parameter estimation errors with mass and time across various scenarios, including single-channel data with multiple modes, multichannel data with the 22 mode, and multichannel data with multiple modes. When only the ringdown signal is considerd, for TianQin, if the total mass is less than $2 \times 10^6 M_\odot$, with the exception of $M_{\rm tot}, q, \iota$ and ϕ_c, all parameters manifest comparable levels of estimation and localization accuracy in both multichannel data with 22-mode and single-channel data with multiple modes. However, when the total mass exceeds $2 \times 10^6 M_\odot$, the accuracy of parameter estimation and localization in single-channel data with multiple modes surpasses that in multichannel data with the 22 mode. Furthermore, this gap will gradually widen as the total mass increases. For LISA, the 22-mode multichannel data and the multimode single-channel data exhibit comparable localization accuracy and parameter estimation error for all parameters except $M_{\rm tot}, q, \iota$ and ϕ_c, which strongly depend on multiple modes. This conclusion remains the same for LISA when the entire IMR signal is taken into consideration. However, for TianQin, when the entire IMR signal is considered, multimode single-channel data consistently provide superior parameter estimation results compared to 22-mode multichannel data, which can gradually increase with higher total mass.

Moreover, by incorporating higher-order modes, we have calculated the improvements in localization accuracy of multichannel data compared to single-channel data and identified that variations in detector results are due to the modulation period of antenna pattern. For TianQin, the multichannel network provides the greatest improvements in localization accuracy for both ringdown and complete IMR signals when the total mass is $2 \times 10^6 M_\odot$, with improvements of more than 2 orders of magnitude and 1 order of magnitude respectively. However, the improvements slightly decrease with other masses. For LISA, the enhancement displays a similar evolutionary trend for both ringdown and complete IMR signals, ranging from less than 1 order of magnitude for the mass of $2 \times 10^5 M_\odot$ to approximately 3 orders of magnitude for the mass of $4 \times 10^7 M_\odot$.

In our study, we examine various combinations of first-generation TDI to investigate its impact on parameter estimation, while assuming that it can effectively eliminate laser frequency noise. Although the use of second-generation TDI may slightly alter the results, our conclusions remain largely unaffected. Additionally, in practical detection scenarios, we may encounter challenges such as orbital perturbations, confusion-foreground noise from Galactic binaries, non-Gaussian noise, and diverse types of overlapping signals that are currently ignored in this study. Finally, the current study is based on data analysis from a single detector and does not consider the potential advantages of utilizing a multidetector network. Exploring the advantages of employing multichannel data under the context of a coherent multidetector operation may be a potential avenue for future research. Overall, a more comprehensive comprehension of the parameter estimation capabilities of detectors or detector networks will aid in establishing more realistic detection targets and understanding the physics underlying sources.

ACKNOWLEDGMENTS

This work was supported by the National Key Research and Development Program of China under Grant No. 2020YFC2201400 and the National SKA Program of China under Grant No. 2020SKA0120300. The authors would like to thank Professors Yungui Gong and Yan Wang for the helpful discussion in the understanding of the parameter estimation for space detectors.

APPENDIX: ORBIT CONFIGURATION OF TIANQIN AND LISA

For TianQin, in the SSB coordinate system, the orbit motion of the satellites can be regarded as the combination of the orbit motion of satellites around the Earth and the orbit motion of the Earth around the Sun. The position of satellites can be presented as [12]

$$\begin{aligned} X_n &= R_d[\cos\phi_s\ \cos\theta_s\ \sin(\alpha_n-\beta_d)+\cos(\alpha_n-\beta_d)\sin\ \phi_s] \\ &+ R_d e_d\left[\frac{1}{2}(\cos 2(\alpha_n-\beta_d)-3)\sin\ \phi_s+\cos(\alpha_n-\beta_d)\cos\phi_s\ \cos\theta_s\ \sin(\alpha_n-\beta_d)\right] \\ &+ \frac{e_d^2}{4}R_d\sin(\alpha_n-\beta_d)[(3\cos 2(\alpha_n-\beta_d)-1)\cos\phi_s\ \cos\ \theta_s-6\ \cos(\alpha_n-\beta_d)\ \sin(\alpha_n-\beta_d)\ \sin\ \phi_s] \\ &+ R\ \cos(\alpha-\beta)+\frac{\mathrm{Re}}{2}(\cos 2(\alpha-\beta)-3)-\frac{3Re^2}{2}\cos(\alpha-\beta)\sin^2(\alpha-\beta), \end{aligned} \tag{A1}$$

$$
\begin{aligned}
Y_n = {} & R_d[\sin\phi_s \cos\theta_s \sin(\alpha_n-\beta_d) - \cos(\alpha_n-\beta_d)\cos\phi_s] \\
& - R_d e_d\left[\frac{1}{2}(\cos 2(\alpha_n-\beta_d)-3)\cos\phi_s - \cos(\alpha_n-\beta_d)\sin\phi_s \cos\theta_s \sin(\alpha_n-\beta_d)\right] \\
& + \frac{e_d^2}{4} R_d \sin(\alpha_n-\beta_d)[(3\cos 2(\alpha_n-\beta_d)-1)\sin\phi_s\cos\theta_s + 6\cos(\alpha_n-\beta_d)\sin(\alpha_n-\beta_d)\cos\phi_s] \\
& + R\sin(\alpha-\beta) + \frac{\mathrm{Re}}{2}\sin 2(\alpha-\beta) + \frac{Re^2}{4}(3\cos 2(\alpha-\beta)-1)\sin(\alpha-\beta),
\end{aligned} \tag{A2}
$$

$$
\begin{aligned}
Z_n = {} & -R_d \sin(\alpha_n-\beta_d)\sin\theta_s - R_d e_d \cos(\alpha_n-\beta_d)\sin(\alpha_n-\beta_d)\sin\theta_s \\
& - \frac{1}{4} e_d^2 R_d (3\cos 2(\alpha_n-\beta_d)-1)\sin(\alpha_n-\beta_d)\sin\theta_s,
\end{aligned} \tag{A3}
$$

where $R_d = 1\times 10^5$ km and e_d (0.005 in this work) are the semimajor axis and eccentricity of the satellite orbit around the Earth, while $R = 1$ AU and $e = 0.0167$ are the semimajor axis and the eccentricity of the Earth orbit around the Sun. $\theta_s = 94.7°$ and $\phi_s = 120.5°$ are the location of RX J0806.3 + 1527, as the reference source targeted by the normal of the TianQin detector plane. $\alpha = 2\pi f_m t + \kappa_0$ is the mean ecliptic longitude of the Earth; $f_m = 1/(1\ \text{year})$ is the angular frequency, and β is the longitude of the perihelion. $\alpha_n = 2\pi f_d t + 2\pi(n-1)/3$ is the orbit phase of the nth satellite in the detector plane, with $f_d = 1/(3.65\ \text{d})$. And β_d is the initial phase.

In the SSB coordinate system, the position of satellites of the LISA program is [11]

$$
\begin{aligned}
X_n &= R(\cos\Psi_n + e)\cos\epsilon\cos\phi_n - R\sqrt{1-e^2}\sin\Psi_n\sin\phi_n \\
Y_n &= R(\cos\Psi_n + e)\cos\epsilon\sin\phi_n + R\sqrt{1-e^2}\sin\Psi_n\cos\phi_n \\
Z_n &= R(\cos\Psi_n + e)\sin\epsilon,
\end{aligned} \tag{A4}
$$

where $R = 1$ AU and e are the semimajor axis and eccentricity of the satellite around the Sun, $e = (1 + 2/\sqrt{3}\alpha + 4/3\alpha^2)^{1/2} - 1$, $\tan\epsilon = \alpha/(1+\alpha/\sqrt{3})$, $\alpha = l/(2R)$, $l = 2.5\times 10^9$ m is the arm length, and $\phi_n = 2\pi/3(n-1)$. And $\Psi_n + e\sin\Psi_n = \Omega t - \frac{2\pi}{3}(n-1) + \Psi_0$, where Ψ_0 and $\Omega = 2\pi/(1\ \text{year})$ are the initial phase and the angular frequency of satellite orbit motion.

[1] R. A. Hulse and J. H. Taylor, A high-sensitivity pulsar survey, Astrophys. J. **191**, L59 (1974).
[2] R. A. Hulse and J. H. Taylor, Discovery of a pulsar in a binary system, Astrophys. J. **195**, L51 (1975).
[3] J. H. Taylor, L. A. Fowler, and P. M. McCulloch, Measurements of general relativistic effects in the binary pulsar PSR1913+16, Nature (London) **277**, 437 (1979).
[4] B. P. Abbott *et al.* (LIGO Scientific and Virgo Collaborations), Observation of gravitational waves from a binary black hole merger, Phys. Rev. Lett. **116**, 061102 (2016).
[5] B. P. Abbott *et al.* (LIGO Scientific and Virgo Collaborations), GWTC-1: A gravitational-wave transient catalog of compact binary mergers observed by LIGO and Virgo during the first and second observing runs, Phys. Rev. X **9**, 031040 (2019).
[6] B. P. Abbott *et al.* (LIGO Scientific and Virgo Collaborations), GWTC-2: Compact binary coalescences observed by LIGO and Virgo during the first half of the third observing run, Phys. Rev. X **11**, 021053 (2021).
[7] K. Danzmann (LISA Study Team), LISA—A ESA cornerstone mission for a gravitational wave observatory, Classical Quantum Gravity **14**, 1399 (1997).
[8] P. Amaro-Seoane *et al.* (LISA Collaboration), Laser interferometer space antenna, arXiv:1702.00786.
[9] W.-R. Hu and Y.-L. Wu, The Taiji program in space for gravitational wave physics and the nature of gravity, Natl. Sci. Rev. **4**, 685 (2017).
[10] J. Luo, L.-S. Chen, H.-Z. Duan, Y.-G. Gong, S. Hu, J. Ji, Q. Liu, J. Mei, V. Milyukov, M. Sazhin, C.-G. Shao, V. T. Toth, H.-B. Tu, Y. Wang, Y. Wang, H.-C. Yeh, M.-S. Zhan, Y. Zhang, V. Zharov, and Z.-B. Zhou, TianQin: A space-borne gravitational wave detector, Classical Quantum Gravity **33**, 035010 (2016).
[11] S. V. Dhurandhar, K. R. Nayak, S. Koshti, and J. Y. Vinet, Fundamentals of the LISA stable flight formation, Classical Quantum Gravity **22**, 481 (2005).
[12] X.-C. Hu, X.-H. Li, Y. Wang, W.-F. Feng, M.-Y. Zhou, Y.-M. Hu, S.-C. Hu, J.-W. Mei, and C.-G. Shao, Fundamentals of the orbit and response for TianQin, Classical Quantum Gravity **35**, 095008 (2018).

[13] B. P. Abbott *et al.* (LIGO Scientific and Virgo Collaborations), Tests of general relativity with GW150914, Phys. Rev. Lett. **116**, 221101 (2016).
[14] B. P. Abbott *et al.* (LIGO Scientific and Virgo Collaborations), GW170817: Observation of gravitational waves from a binary neutron star inspiral, Phys. Rev. Lett. **119**, 161101 (2017).
[15] C. L. Fryer, D. E. Holz, and S. A. Hughes, Gravitational wave emission from core collapse of massive stars, Astrophys. J. **565**, 430 (2002).
[16] C. L. Fryer and K. C. B. New, Gravitational waves from gravitational collapse, Living Rev. Relativity **6**, 2 (2003).
[17] S. Woosley and J. Bloom, The supernova–gamma-ray burst connection, Annu. Rev. Astron. Astrophys. **44**, 507 (2006).
[18] W. H. Lee and E. Ramirez-Ruiz, The progenitors of short gamma-ray bursts, New J. Phys. **9**, 17 (2007).
[19] K. Belczynski, R. O'Shaughnessy, V. Kalogera, F. Rasio, R. E. Taam, and T. Bulik, The lowest-mass stellar black holes: Catastrophic death of neutron stars in gamma-ray bursts, Astrophys. J. **680**, L129 (2008).
[20] C. L. Fryer, K. Belczynski, E. Ramirez-Ruiz, S. Rosswog, G. Shen, and A. W. Steiner, The fate of the compact remnant in neutron star mergers, Astrophys. J. **812**, 24 (2015).
[21] D. E. Holz and S. A. Hughes, Using gravitational-wave standard sirens, Astrophys. J. **629**, 15 (2005).
[22] B. P. Abbott *et al.* (LIGO Scientific and Virgo Collaborations), A gravitational-wave standard siren measurement of the Hubble constant, Nature (London) **551**, 85 (2017).
[23] C. Cutler and E. E. Flanagan, Gravitational waves from merging compact binaries: How accurately can one extract the binary's parameters from the inspiral waveform?, Phys. Rev. D **49**, 2658 (1994).
[24] L. Wen and B. F. Schutz, Coherent network detection of gravitational waves: The redundancy veto, Classical Quantum Gravity **22**, S1321 (2005).
[25] R. N. Lang and S. A. Hughes, Localizing coalescing massive black hole binaries with gravitational waves, Astrophys. J. **677**, 1184 (2008).
[26] M. van der Sluys, V. Raymond, I. Mandel, C. Röver, N. Christensen, V. Kalogera, R. Meyer, and A. Vecchio, Parameter estimation of spinning binary inspirals using Markov Chain Monte Carlo, Classical Quantum Gravity **25**, 184011 (2008).
[27] S. Fairhurst, Triangulation of gravitational wave sources with a network of detectors, New J. Phys. **11**, 123006 (2009).
[28] S. Fairhurst, Source localization with an advanced gravitational wave detector network, Classical Quantum Gravity **28**, 105021 (2011).
[29] S. Nissanke, J. Sievers, N. Dalal, and D. Holz, Localizing compact binary inspirals on the sky using ground-based gravitational wave interferometers, Astrophys. J. **739**, 99 (2011).
[30] K. Grover, S. Fairhurst, B. F. Farr, I. Mandel, C. Rodriguez, T. Sidery, and A. Vecchio, Comparison of gravitational wave detector network sky localization approximations, Phys. Rev. D **89**, 042004 (2014).
[31] J. W. Armstrong, F. B. Estabrook, and M. Tinto, Time-delay interferometry for space-based gravitational wave searches, Astrophys. J. **527**, 814 (1999).
[32] F. B. Estabrook, M. Tinto, and J. W. Armstrong, Time-delay analysis of LISA gravitational wave data: Elimination of spacecraft motion effects, Phys. Rev. D **62**, 042002 (2000).
[33] M. Tinto and S. V. Dhurandhar, Time-delay interferometry, Living Rev. Relativity **17**, 6 (2014).
[34] M. Peterseim, O. Jennrich, and K. Danzmann, Accuracy of parameter estimation of gravitational waves with LISA, Classical Quantum Gravity **13**, A279 (1996).
[35] M. Peterseim, O. Jennrich, K. Danzmann, and B. F. Schutz, Angular resolution of LISA, Classical Quantum Gravity **14**, 1507 (1997).
[36] C. Cutler, Angular resolution of the LISA gravitational wave detector, Phys. Rev. D **57**, 7089 (1998).
[37] T. A. Moore and R. W. Hellings, Angular resolution of space-based gravitational wave detectors, Phys. Rev. D **65**, 062001 (2002).
[38] A. Vecchio and E. D. L. Wickham, Effect of the LISA response function on observations of monochromatic sources, Phys. Rev. D **70**, 082002 (2004).
[39] K. G. Arun, B. R. Iyer, B. S. Sathyaprakash, S. Sinha, and C. VanDenBroeck, Higher signal harmonics, LISA's angular resolution, and dark energy, Phys. Rev. D **76**, 104016 (2007).
[40] E. K. Porter and N. J. Cornish, Effect of higher harmonic corrections on the detection of massive black hole binaries with LISA, Phys. Rev. D **78**, 064005 (2008).
[41] A. Błaut, Accuracy of estimation of parameters with LISA, Phys. Rev. D **83**, 083006 (2011).
[42] W.-H. Ruan, C. Liu, Z.-K. Guo, Y.-L. Wu, and R.-G. Cai, The LISA-Taiji network, Nat. Astron. **4**, 108 (2020).
[43] W.-H. Ruan, C. Liu, Z.-K. Guo, Y.-L. Wu, and R.-G. Cai, The LISA-Taiji network: Precision localization of coalescing massive black hole binaries, Research **2021**, 6014164 (2021).
[44] G. Wang, W.-T. Ni, W.-B. Han, S.-C. Yang, and X.-Y. Zhong, Numerical simulation of sky localization for LISA-Taiji joint observation, Phys. Rev. D **102**, 024089 (2020).
[45] W.-F. Feng, H.-T. Wang, X.-C. Hu, Y.-M. Hu, and Y. Wang, Preliminary study on parameter estimation accuracy of supermassive black hole binary inspirals for TianQin, Phys. Rev. D **99**, 123002 (2019).
[46] S.-J. Huang, Y.-M. Hu, V. Korol, P.-C. Li, Z.-C. Liang, Y. Lu, H.-T. Wang, S. Yu, and J. Mei, Science with the TianQin observatory: Preliminary results on galactic double white dwarf binaries, Phys. Rev. D **102**, 063021 (2020).
[47] C. Zhang, Y. Gong, H. Liu, B. Wang, and C. Zhang, Sky localization of space-based gravitational wave detectors, Phys. Rev. D **103**, 103013 (2021).
[48] C. Zhang, Y. Gong, B. Wang, and C. Zhang, Accuracy of parameter estimations with a spaceborne gravitational wave observatory, Phys. Rev. D **103**, 104066 (2021).
[49] C. Zhang, Y. Gong, and C. Zhang, Parameter estimation for space-based gravitational wave detectors with ringdown signals, Phys. Rev. D **104**, 083038 (2021).
[50] C. Zhang, Y. Gong, and C. Zhang, Source localizations with the network of space-based gravitational wave detectors, Phys. Rev. D **106**, 024004 (2022).
[51] S. Marsat, J. G. Baker, and T. D. Canton, Exploring the Bayesian parameter estimation of binary black holes with LISA, Phys. Rev. D **103**, 083011 (2021).

[52] N. J. Cornish and S. L. Larson, Space missions to detect the cosmic gravitational-wave background, Classical Quantum Gravity **18**, 3473 (2001).
[53] L. Blanchet, Gravitational radiation from post-Newtonian sources and inspiralling compact binaries, Living Rev. Relativity **17**, 2 (2014).
[54] C. García-Quirós, M. Colleoni, S. Husa, H. Estellés, G. Pratten, A. Ramos-Buades, M. Mateu-Lucena, and R. Jaume, Multimode frequency-domain model for the gravitational wave signal from nonprecessing black-hole binaries, Phys. Rev. D **102**, 064002 (2020).
[55] K. Wette, SWIGLAL: Python and Octave interfaces to the LALSuite gravitational-wave data analysis libraries, SoftwareX **12**, 100634 (2020).
[56] A. Nitz *et al.*, GWASTRO/PyCBC: V2.1.2 release of PyCBC, 10.5281/zenodo.7885796 (2023).
[57] V. Varma and P. Ajith, Effects of nonquadrupole modes in the detection and parameter estimation of black hole binaries with nonprecessing spins, Phys. Rev. D **96**, 124024 (2017).
[58] J. Calderón Bustillo, P. Laguna, and D. Shoemaker, Detectability of gravitational waves from binary black holes: Impact of precession and higher modes, Phys. Rev. D **95**, 104038 (2017).
[59] G. Pratten, P. Schmidt, H. Middleton, and A. Vecchio, Precision tracking of massive black hole spin evolution with LISA, arXiv:2307.13026.
[60] N. J. Cornish and R. W. Hellings, The effects of orbital motion on LISA time delay interferometry, Classical Quantum Gravity **20**, 4851 (2003).
[61] D. A. Shaddock, M. Tinto, F. B. Estabrook, and J. W. Armstrong, Data combinations accounting for LISA spacecraft motion, Phys. Rev. D **68**, 061303 (2003).
[62] M. Tinto, F. B. Estabrook, and J. W. Armstrong, Time delay interferometry with moving spacecraft arrays, Phys. Rev. D **69**, 082001 (2004).
[63] T. A. Prince, M. Tinto, S. L. Larson, and J. W. Armstrong, LISA optimal sensitivity, Phys. Rev. D **66**, 122002 (2002).
[64] M. Vallisneri, J. Crowder, and M. Tinto, Sensitivity and parameter-estimation precision for alternate LISA configurations, Classical Quantum Gravity **25**, 065005 (2008).
[65] T. Robson, N. J. Cornish, and C. Liu, The construction and use of LISA sensitivity curves, Classical Quantum Gravity **36**, 105011 (2019).
[66] M. Vallisneri, Use and abuse of the Fisher information matrix in the assessment of gravitational-wave parameter-estimation prospects, Phys. Rev. D **77**, 042001 (2008).
[67] C. Cutler, Angular resolution of the LISA gravitational wave detector, Phys. Rev. D **57**, 7089 (1998).
[68] P. Jaranowski and A. Królak, Gravitational-wave data analysis. Formalism and sample applications: The Gaussian case, Living Rev. Relativity **15**, 4 (2012).
[69] Planck Collaboration *et al.*, Planck 2018 results. VI. Cosmological parameters, Astron. Astrophys. **641**, A6 (2020).